INVESTIGATION OF MICROALGAE GASIFICATION IN A BUBBLING BED GASIFIER WITH INTEGRATED SOLID OXIDE FUEL CELL USING ASPEN PLUS

Senem SEZER and Uğur ÖZVEREN*

Department of Chemical Engineering, Marmara University, Istanbul 34722, Turkey
*Corresponding author. Email: ugur.ozveren@marmara.edu.tr

ABSTRACT

High-temperature solid oxide fuel cells (SOFCs) provide sustainable and highly efficient distributed and modular energy conversion systems when combined with biomass gasification. Biomass gasification is an efficient alternative to the use of fossil fuels for the production of syngas containing mainly H_2, CO, and CH_4. Compared to inland biomass sources, microalgae are considered a promising source due to their more flexible cultivation methods, higher growth rate, and lower land requirements. They can be grown in the ocean, freshwater, or wastewater without requiring land for agriculture. By using steam as a gasification agent, the gasifier produces a higher hydrogen content in the syngas, resulting in a suitable fuel for SOFC. This study was conducted in Aspen Plus simulation to investigate the gasification with integrated SOFC system using microalgae as biomass source. A bubbling fluidized bed gasifier was selected and integrated into the SOFC after cleaning of the syngas. As a result, the influence of various key parameters such as energy efficiency, voltage and current density depending on the operating temperature of the gasifier and anode, and the ratio of steam to biomass of the gasifier in an integrated biomass gasification and SOFC is investigated. The results show that the efficiency of the system increases dramatically as the concentration of H_2 increases, but it decreases considerably when the concentrations of CO and CO_2 increase.

Keywords: Biomass**,** SOFC, Syngas, Gasifier, Energy Efficiency

1. Introduction

In the following decades, global energy consumption will continue to climb at a quick rate (Indrawan, 2018). With a considerable rise in population, there will be a proportional increase in demand for trustworthy and sustainable energy supplies. Fossil fuel depletion is posing a serious danger to economic development and energy security (Celaya et al., 2015). As a result, the use of alternative energy sources to replace traditional fuels is gaining popularity. Biomass is an attractive alternative from an environmental standpoint because of its CO_2 neutrality and low nitrogen and sulfur content. Biomass, unlike fossil fuels, is rapidly replenished and contains a diverse range of waste products obtained from animals and plants (Shayan et al., 2018).

Microalgae have more flexible culture methods, faster growth rates and need less area than terrestrial plants (Chen et al., 2011). Furthermore, since crops and algae do not compete, algae production will have no detrimental influence on food costs or other human activities. Algae might be treated thermochemically to create energy or biofuel in addition to biological conversion (López-González et al., 2014). Microalgal biomass has lower decomposition temperatures during the thermal conversion process than lignocellulosic biomass, resulting in better reactivity and reduced operating costs. The changes in composition are the primary cause. Proteins, lipids, and carbohydrates are the key components of microalgae, which are less thermally resistant than hemicellulose, cellulose and notably lignin, which are the main components of lignocellulosic biomass (Chisti, 2007). One of the thermochemical methods for algae to create value added products is via gasification.

Through partial oxidation with air, steam, or CO_2, gasification of algae might produce a syngas consisting of CO_2, CH_4, H_2, and CO (Safarian et al., 2020). Gasification is a successful approach because it increases energy recovery, provides less CO_2 emissions, and reduces tar and char content in the finished product.

The operating and design characteristics of the gasification, like heat source, gasifier type, gasification agent, and pressure, are the most important variables for achieving the proper syngas composition. For more effective syngas production, selecting the appropriate gasifier type is crucial. Fluidized bed is favoured over entrained flow and fixed bed gasifiers because of its improved heat transfer and mass transfer, higher carbon conversion efficiency, and ability to utilize a broad range of particle sizes (Gómez-Barea & Leckner, 2010). Fluidized bed gasifiers may either

circulate the gas or bubble up through the bed. The BFBG is a very simple machine for producing syngas. When using a different oxidizing agent, the exit gas will have different chemical and physical properties. When steam is applied as an gasifying agent, it creates a syngas with a greater H_2 content.

Electricity and heat might be produced directly in an steam turbine, gas turbine, or fuel cells using syngas (Segurado et al., 2019). It is widely agreed that fuel cell-based systems are among the most viable of the many possible combined process systems for producing electricity from syngas. Electrochemical machines known as fuel cells convert chemical energy into electricity with great efficiency and little pollution. One form of fuel cell that can be run at high temperature than others is the solid oxide fuel cell (SOFC). Since a higher processing temperature helps to fuel adaptability and contaminant tolerance, this kind is also considered the most practicable for biomass-derived fuels.

Although the combined gasification and SOFC system has the potential to be more efficient than competing heat and power technologies, more research and optimization are required to address issues with the system's design and operation. To define the influence of the operational parameters on the integrated system, more time and money are needed for experiments. As such, gasification and SOFC unit modeling is a dependable method for determining the best setup and optimal values for operating circumstances (Ahmed et al., 2012; Hauck et al., 2017). The thermodynamic (zero-dimensional) approach is often used in modeling-related research withouth to need gasifier design (Basu, 2018; Silva et al., 2019). Thermodynamic modeling is the most straightforward approach to making such estimates (Patra & Sheth, 2015). The gasification process and the SOFC are shown as a sequence of complicated chemical processes.

Aspen Plus is commonly used as the modeling tool of choice for designing systems based on mass balance and energy balance (Ramos et al., 2019). Since the integrated gasification and SOFC model was developed with thermodynamic principles in mind, it is possible to acquire the output parameters with ease and precision, including cell power, cell voltage, efficiency, syngas composition, and so on. A thermodynamic equilibrium-based approach might be either stoichiometric or non-stoichiometric. The stoichiometric model is based on the mass-action law and the equilibrium constants. For a simulation model to be run using the stoichiometric approach, the conversion rates of chemical processes and the stoichiometric coefficients of each component

must be specified. Conversely, the non-stoichiometric approach based on Gibbs free energy reduction is applicable in every situation because of its generality (Basu, 2018; Żogała, 2014). Another benefit of the non-stoichiometric approach is that it may be used to carry out chemical reactions using simply the chemical formula of the reactants, without the need of knowing anything about reaction kinetics, conversion values or stoichiometric coefficients (Baruah & Baruah, 2014).

Some research has simulated biomass gasification and integrated systems via Aspen Plus using the Gibbs free energy minimization concept. Lopes-Motta *et al.* (Motta et al., 2019) studied the impact of operating parameters and gasifying agent (steam and oxygen) on syngas composition and process performance using Aspen Plus. Numerous scenarios of biomass gasification in diverse fluidized bed configurations were simulated based on Gibbs free energy minimization approach. Faraji and Saidi (Faraji & Saidi, 2021) used Aspen Plus to create a steady-state model of algal biomass gasification. Algal waste, Rhizoclonium sp, Chlorella vulgaris and Spirogyra were chosen as the algal biomass feedstock, and a sensitivity analysis was conducted to determine the effect of gasifier pressure, gasifier temperature and air flow rate on the composition of syngas. The results of this research were utilized to make predictions about the behavior of the process at commercial and industrial sizes, allowing for its efficient and economical industrialisation. Lan *et al.* (Lan et al., 2018) built a model of the gasification-gas turbine system based on Gibbs free energy minimization using the ASPEN PLUS simulation environment to forecast the gasifier's performance and power generating capacity under different operating circumstances. The developed model succesffully validated and model run with high accuracy. Palomba *et al.* (Palomba et al., 2017) obtained the syngas from the gasification of lignocellulosic biomass and used it for heating and electricity production in Aspen Plus simulation environment. They validated all components and developed the gasification-SOFC model to obtain CHP and plant gross electrical and efficiencies.

Even though there is a lot of work related to gasification, microalgae gasification, combined gasification and power processes, there is no model developed for the gasification with integrated SOFC process using algal biomass as fuel using Aspen Plus simulation. In this study, for the first time, a developed bubbling fluidized bed gasifier-SOFC model from literature was used to conduct an integrated microalgae gasification and SOFC process. The model was validated with experimental work and the effects of operating parameters such as gasifier temperature, steam to

biomass ratio of the gasifier and anode temperature were discussed in terms of electrical efficiency (E), voltage (V) and current density (I).

2. Methodology

2.1. Material Characterization

In this work, microalgae were selected as a marine biomass sample to use as a feedstock, and their physicochemical parameters were gathered from the existing literature. Microalgae, unlike land plants, may develop without a soil base, a central stem, or leaves. Microalgae samples with an LHV (dry basis) of 14.75 MJ/kg were selected for the gasification process due to their favorable energy properties. Table 1 displays the findings of both the proximate and ultimate analyses performed on the microalgae. Microalgae's hydrogen, carbon, sulphur, and nitrogen levels were measured experimentally, while oxygen was found by a difference calculation.

Table 1. Proximate and ultimate analyses of Hapalosiphon sp. microalgae (Liu et al., 2012).

Proximate Analysis (wt.%)	Volatile Matter	74.29
	Ash	13.98
	Moisture	3.97
	Fixed Carbon	11.73
Ultimate Analysis (wt.%)	Oxygen	37.59
	Nitrogen	6.45
	Hydrogen	7.44
	Carbon	47.94
	Sulfur	0.58

As seen in Table 1. Hapalosiphon sp. microalgae has exceptable amount of C, H and O content for gasification with integrated SOFC system.

2.2. Model Discription

This section details the work done using the Aspen Plus simulation tool to create a model of a gasification with integrated SOFC. In order to mimic complicated systems in Aspen Plus, they are often divided into smaller subprocesses. It's important to depict each individual process step to be as realistic as desirable. To clear away each step, we use a sequential modular strategy. It is challenging to describe the gasification with integrated SOFC system because of the many specific types of chemical reactions that occur throughout the process (exothermic and endothermic, homogeneous and heterogeneous).

The equilibrium model is a basic tool for modeling and predicting a system's output. The gasification with integrated SOFC system was modeled in the literature using the thermodynamic equilibrium model in Aspen Plus program (V11 aspenONE Engineering Suite) (Sezer et al., 2022). The following assumptions were taken into account throughout the simulation of the process in order to create a reliable model:

- The procedure has developed in steady state conditions.
- There are zero pressure and heat losses.
- The fuel devolatilizes instantly.
- Char is entirely made of carbon.
- Ash is nonreactive because of its presumed inertness.
- Chemical equilibrium is attained within a practical amount of time.
- H_2, CO_2, CO, H_2O, CH_4 and some of the heavyhydrocarbons are found in syngas.
- Chlorine (Cl) and sulfur (S) found in biomass combine to generate hydrogen chloride (HCl) and hydrogen sulfide (H_2S), respectively.
- Gases are thought to be ideal.
- Only nitrogen (N_2) and oxygen (O_2) make up the air.

Figure 1 shows the Aspen Plus flow diagram for the gasification with integrated SOFC model

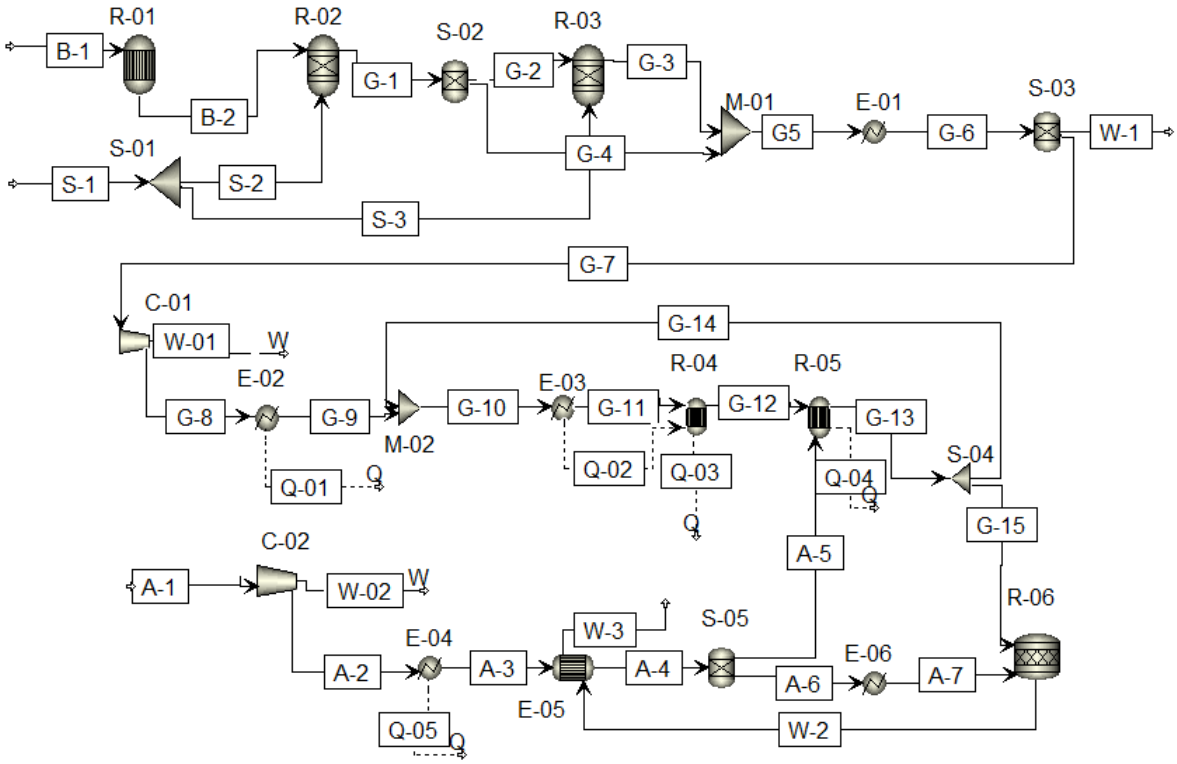

Figure 1. Process flow diagram of the gasification with integrated SOFC system (Sezer et al., 2022).

From receiving the fuel until completing the syngas generation, the whole gasification process was shown. In addition, the syngas from the gasifier was used as the fuel for SOFC, which then used Fortran subroutine computations to generate power. Using distinct reactors and building components, we were able to describe in great detail each stage of the process. Due to the rapid and complicated nature of the gasification processes and the intricate configuration of SOFC, equilibrium-based models were favored to be simplify matters and developed using by minimization of the Gibbs free energy (non-stoichiometric).

2.2.1. Bubbling Fluidized Bed Gasifier Part

Drying, pyrolysis, combustion, and reduction are the four cornerstone steps of the gasification process; they are modeled by connecting unit operation blocks in a sequential manner. Inputs for the fuel's thermodynamic characteristics and flow rate were made after the sample was defined as a nonconventional component based on findings from both ultimate and proximate analyses. The biomass must be transformed into a conventional form in a yield reactor called “R-01”. The

following “R-02” block's (RGIBBS reactor) purpose is carrying out the drying and pyrolysis steps. The temperature at this stage is typically set about 200 and 500 °C. Here, pyrolysis, the second stage of thermal degradation, was initiated by setting the temperature to 300 °C. Because water and other volatiles may be released throughout the pyrolysis process, it was unnecessary to model drying as a distinct step.

Compared to other gasifying agents, steam produces a syngas with a higher H_2 content, hence it was favored. Pure steam flow “S-1” was first implemented in the “S-01” block, operating at 250 °C and atmospheric pressure. The entering steam flow was split into two streams at a predetermined ratio to provide a steam environment inside the pyrolysis and gasification reactors. The thermodynamic conditions of the “S-1” were not altered when it was sent “R-02” reactor. Gas and solid phase processes of the “R-02” reactor produced the output stream “G-1”, which mostly consisted of CH_4, H_2O, CO_2 and tiny amounts of CO, C_2H_6 and C_2H_2. It was decided to split some of the CH_4 and put in the “S-02” block so that it wouldn't all be used up. The CH_4 achieves a chemical equilibrium and is not detectable in the syngas because of the high temperature in the “R-03” reactor. Additionally, the “S-02” block was used to separate gases that do not participate in the gasification operations. The gasification processes were carried out in “R-03” reactor. The G-4 that was collected was piped directly into the exhaust stream, bypassing the gasification unit entirely.

The key gasification and oxidation reactions—the water–gas shift, steam–methane reforming and Boudouard —occur in the gasification section. After passing through the “G-2” stream, the “R-03” reactor heats up to well over 700 °C to carry out the reactions in accordance with the concept of minimization of Gibbs free energy. Using the secondary “S-3” stream, pure steam at the identical thermodynamic values as the intake steam (atmospheric pressure and 250 °C) was injected into the “R-03” reactor.

At the equal temperature as the “R-03” reactor, syngas was generated together with water and other by-products. The “G-3” outflow stream was mixed with the “G-4” stream after being separated from “G-1” in the pyrolysis process using the “M-01” mixer. The gas mixture at 500 °C was obtained by passing “G-6” through a “E-01” block. Moisture and undesirable byproducts (H_2S, N_2, ash, etc.) should be cleaned from this flow. To do this, we employed the “S-03” block's

separation procedure to generate the “G-7” stream, which consisted only of the gases H_2, CH_4, CO and CO_2. Table 2 details the various building components and reactors in this part.

Table 2. Definition of reactors and blocks in the gasification part.

Name	Block	Description
R-01	RYIELD	Biomass is converted into conventional form.
R-02, R-03	RGIBBS	Pyrolysis and gasification steps occur in these reactors.
S-01	FSPLIT	Steam is divided between the two reactors.
M-01	MIXER	G3 and S-GAS streams are mixed.
E-01	HEATER	Cools the gas to desired temperature
E-05	HEATX	Temperature is maintained as 500 °C
S-02, S-03	SEP	Predetermined amount of gases is separated.

2.2.2. SOFC Part

Aspen Plus with Fortran subroutines were used to conduct the SOFC model and calculate the desired parameters such as voltage, current density and energy efficiency. When taking into account its cutting-edge technology and its potential for commercialisation, the tubular SOFC system stands out as the most promising. For the purposes of this research, a Siemens Power Generation Inc.-developed 120 kW tubular SOFC unit was chosen for analysis. Many authors have cited this method's usage in their work (Doherty et al., 2010; Özveren, 2013; Zhang et al., 2005).

For the purpose of maintaining a constant pressure in the fuel supply, the “G-7” stream was sent through the “C-01” compressor block. Discharge pressure was determined by setting the design specification block “D-1” to a P_{SYNGAS}/P_{SOFC} ratio of 3. The “G-7” temperature, composition and pressure were defined, but the starting flow rate was adjusted according to the obtaining desired stack power using design specification block “D-5”.

Compressed stream (G-8) was preheated by block “E-02”, supplied to “M-02”, and mixed with “G-14”, the recycle from the “ANODE (G-13)” output. The “R-04” and “E-03” worked together to depict the SOFC stack's pre-reformer. The primary objective of “E-03” is to provide the

necessary heat for carrying out the reforming reactions in “R-04”, and this is accomplished by using the heat emitted during the cooling process. When the net heat duty of the “R-04” is being equal zero value, as it is when run adiabatically, the discharge stream temperature of the “G-11” is adjusted using “E-03”.

It is expected that only H_2 may participate in electrochemical processes, the "R-04" reactor converts CO into H_2 ($CO + H_2O \leftrightarrow CO_2 + H_2$) and other heavier hydrocarbons and CH_4 into H_2 ($C_xH_z + xH_2O \leftrightarrow (z/2 + x)\, H_2 + xCO$). At that point, “G-12” stream combines with the O_2 flow coming from the “S-05” as it runs along the “R-05” reactor. Since ion transfer cannot be simulated with the existing model, just a single full reaction was carried out for the oxidant and fuel streams ($H_2 + 0.5O_2 \rightarrow H_2O$).

The air was introduced into the system through the “C-02” block, which is a kind of air compressor. The air discharge pressure was adjusted to be somewhat greater than the surrounding atmosphere. Its composition, as well as its pressure and temperature, were entered. The design specification block “D-4” was used to set the air molar flow rate at a value that would result in an air utilization factor named as U_a of 0.19. The “E-05” heat exchanger block was used to bring the “A-2” stream from compressor stream up to the preheating temperature of air. The combustion processes in the “R-06” reactor produced hot products that provided the necessary heat. The required temperature and pressure of air is introduced into the “S-05” block. The “S-05” module filters out the O_2 in the air. The calculator block partitioned the O_2 fraction and organized it is obtaining a desired amount O_2 by using following equations:

$$nH_{2,in} = nH_{2,syngas} + 1\,(nCO_{syngas}) + 4\,(nCH_{4,syngas}) + \ \ldots \tag{1}$$

$$Uf = \frac{nH_{2,cons}}{nH_{2,in}} \tag{2}$$

$$nO_{2,cons} = 0.5nH_{2,cons} \tag{3}$$

$$O_{2,split} = \frac{nO_{2,cons}}{nO_{2,in}} \tag{4}$$

Using the value of 0.85 for the fuel utilization factor (U_f), we can get the total molar flow rate of $H_{2,cons}$.

A fixed quantity of O_2 from the cathode was used to complete the reaction in the anode reactor. Then, utilizing design-spec "D-2" a fraction of the "R-05" gas was recycled, with the ratio being set at 1.8 with regard to the steam to carbon ratio. The stoichiometric reactor "R-06" burned any remaining "R-05" fuel with any extra "S-05" oxidant. The air was preheated by the combustion products in the "E-05" before it entered the "S-05" block. Furthermore, the exhaust stream temperature from the stack was defined.

Table 3 provides the operation blocks.

Table 3. Outlined of components in the SOFC.

Block Name	Block Type	Description
C-01, C-02	COMPR	Sets the operational pressure of streams.
E-02, E-03, E-04, E-06	HEATER	Sets the temperature in streams.
M-02	MIXER	Mixes the streams.
R-04, R-05	RGIBBS	Reforms the other hydrocarbons and methane to H_2, represents the electrochemical parts.
S-05	SEP	Separates the O_2.
S-04	FSPLIT	Splits the stream to acquire the required steam to carbon ratio.
R-06	RSTOIC	Represents the combustion processes.
E-05	HEATX	Heats the air stream.

2.2.2.1.Calculations of SOFC Parameters

The voltage calculation begins with an assumption of ideal performance. Next, the real voltage is determined by calculating the voltage losses in light of the non-ideal behavior. The expression of the standard potential when the voltage present in standard pressure is the ideal voltage value (V_{ideal}) (O'Hayre et al., 2009):

$$V_{id} = \frac{-\Delta \overline{g_f}}{2F} \quad (5)$$

Maximum electrical energy produced by a fuel cell without losses is represented by the Gibbs free energy of formation ($\Delta\bar{g}_f$) (Song, 2002). The anode half-reaction releases 2 moles of electrons, where F is the Faraday constant (96485 C/mol). Cell voltage is found to be most closely approximating the Nernst voltage (V_{Nernst}), sometimes called the reversible or equilibrium potential. The V_{Nernst} is calculated using the Nernst equation as seen in below:

$$V_{Nr} = V_{id} + \frac{RT}{2F} ln \frac{P_{H_2} P_{O_2}^{0.5}}{P_{H_2O}} \quad (6)$$

The equations in Table 4 may be used to determine the activation, concentration and ohmic losses that contribute to the overall voltage drop.

Table 4. Calculation of voltage losses.

Activation ($V_{activation}$)		Eq.
Cathode	$\frac{1}{R_{A,Cathode}} = \frac{4F}{R_g T_{OP}} k_{CA} \left(\frac{P_{O_2}}{P^0}\right)^m exp\left(\frac{-E_{CA}}{R_g T_{OP}}\right)$	(7)
Anode	$\frac{1}{R_{A,Anode}} = \frac{2F}{R_g T_{OP}} k_{AN} \left(\frac{P_{H_2}}{P^0}\right)^m exp\left(\frac{-E_{AN}}{R_g T_{OP}}\right)$	(8)
Ohmic (V_{ohmic})		
Electrolyte	$V_{O,Elect} = j\rho_E t_E$	(9)
Interconnection	$V_{O,Inter} = j\rho_{Int} \frac{t_{Int}}{w_{Int}} (\pi D_{mA})$	(10)
Cathode	$V_{O,Cathode} = \frac{j\rho_{CA}(\pi D_{mA})^2}{8t_C} A[A + 2(1 - A - B)]$	(11)
Anode	$V_{O,Anode} = \frac{j\rho_{AN}(A\pi D_{mA})^2}{8t_A}$	(12)
Concentration (V_{conc})		
Cathode	$V_{C,cathode} = \frac{R_g T_{OP}}{4F} ln\left[\frac{(P_{SOFC}/\delta_{O_2}) - \left[(P_{SOFC}/\delta_{O_2}) - y^0_{O_2} P_{SOFC}\right] exp\left[(R_g T_{OP}/4F)(\delta_{O_2} t_C / D_{C,eff} P_{SOFC}) j\right]}{y^0_{O_2} P_{SOFC}}\right]$	(13)
Anode	$V_{C,anode} = \frac{R_g T_{OP}}{2F} ln\left[\frac{1 - (R_g T_{OP}/2F)(t_A / D_{A,eff} y^0_{H_2} P_{SOFC}) j}{1 + (R_g T_{OP}/2F)(t_A / D_{A,eff} y^0_{H_2O} P_{SOFC}) j}\right]$	(14)

The all terms related to voltage losses and cell geometry and material characteristics are presented in Table 5 and 6, respectively.

Table 5. Model parameters related to voltage losses.

Activation	
m (slope)	0.25
k_A (A/m^2)	2.13×10^{8}
k_B (A/m^2)	1.49×10^{10}
E_C (J/mol)	160000
E_A (J/mol)	110000
Ohmic	
A	0.804
B	0.13
Concentration	
ε	0.5
r (m)	5×10^{-7}
∃	5.9

Table 6. Model geometry and material parameters.

Geometry	
Cell Length (m)	1.5
Cell Diameter (m)	0.022
w_{Int} (m)	0.009
t_{Int}, t_A, t_E, t_C (m)	0.000085, 0.0001, 0.00004, 0.0022
Material Characteristics	
ρ_{Anode} (Ω m)	$2.98\times10^{-5}\exp(-1392/T_{OP})$
ρ_{Int} (Ω m)	0.025
ρ_E (Ω m)	$2.94\times10^{-5}\exp(10350/T_{OP})$
$\rho_{Cathode}$ (Ω m)	$8.114\times10^{-5}\exp(600/T_{OP})$

Concentration loss (V_{conc}) occurs in porous electrodes due to limitations in mass transport. We assumed diffusion and convection in the electrodes, and used the corresponding equations in Table 7 to get the relevant values.

Table 7. Diffusion calculations

Parameters	**Eq.**
$D_{K,eff} = D_K(\varepsilon/\exists)$	(15)
$D_K = 97r(T_{OP}/M_i)^{0.5}$	(16)
$D_{ik} = \frac{1\times10^{-7}T_{OP}^{1.75}(1/M_i+1/M_k)^{1/2}}{P(v_i^{1/3}+v_k^{1/3})^2}$	(17)
$D_{ik,eff} = D_{ik}(\varepsilon/\exists)$	(18)
$1/D_{i,eff} = 1/D_{ik,eff} + \frac{1}{D_{K,i,eff}}$	(19)
$D_{A,eff} = D_{H_{2,eff}}\left(\frac{y_{H_2O}^0 P_{SOFC}}{P_{SOFC}}\right) + D_{H_2O,eff}\left(\frac{y_{H_2}^0 P_{SOFC}}{P_{SOFC}}\right)$	(20)
$D_{C,eff} = D_{O_{2,eff}}$	(21)
$\delta_{O_2} = \frac{D_{K,O_{2,eff}}}{D_{K,O_{2,eff}}+D_{O_2-N_{2,eff}}}$	(22)

To get the actual voltage (V_{real}), the following equation was used:

$$V_{real} = V_{Nernst} - (V_{ohmic} + V_{conc} + V_{actual}) \quad (23)$$

The following equations can be used to determine the current (I) and the current density (j), on the basis of the amount of H_2 used in electrochemical processes:

$$I = 2 * F * (H_{2,cons} * \frac{1000}{3600}) \quad (24)$$

$$j = \frac{I}{A} \quad (25)$$

F is Faraday constant and active area (A).

Using the information about the fuel (LHV_{fuel}) that is supplied into the SOFC and the information about the AC power (AC_{power}) that is fed into the SOFC, a Fortran codes in the D-5 design-spec was able to determine the electrical efficiency (E) of the SOFC. Using the following equation, we can get E after converting DC power (DC_{power}) to AC_{power} with an efficiency of 0.92:

$$E = \frac{DC_{power} * 0.92}{1000} / \mathrm{LHV}_{fuel} \times 100$$

3. Results

3.1. Bubbling Fluidized Bed Gasifier Model Validation

After BFBG model creation is complete, the model's correctness must be validated. Two independent experimental data sets from the published research were used to validate the developed process. The experimental conditions presented in Table 7 were used to input the system's operational parameters, fuel sample, and gasification agents' flow rates.

Table 8. Conditions in which the experiments were conducted

	Experimental - 1 (Loha et al., 2013)	**Experimental - 2 (Lv et al., 2003)**
Fuel Type	Rice Husk	Pine Sawdust
Gasifier Temperature (°C)	850	800
Fuel Feed Flow (kg/h)	2.5	0.445
Equivalence Ratio	0.35	0.22
Steam to Biomass Ratio	0.5	1.35
Gasification Agent	Steam, Air	Steam, Air

The first set of experiments used rice husk as fuel, whereas the second set of experiments utilized pine sawdust. In both cases, researchers found that combining air and steam (in varying proportions) was used as gasifying agent. Molar fraction of syngas for CH_4, H_2, CO_2 and CO were evaluated after simulating under the same operating circumstances as experiments, and the results are presented in Table 9 and 10.

Table 9. Comparison of syngas composition from our model and first experimental study

Component	Our Model	Experimental-1 (Loha et al., 2013)
CO	14.50	14.80
CO_2	18.40	18.90
H_2	12.30	12.40
CH_4	3.00	1.90

Table 10. Comparison of syngas composition from our model and second experimental study

Component	Our Model	Experimental-2 (Lv et al., 2003)
CO	40.35	41.61
CO_2	16.85	17.53
CH_4	8.34	10.05
H_2	29.78	30.79

It was found via comparison that the model performs effectively even when mole fractions vary by a little amount. These variations in outcomes are consistent with those seen in earlier research investigations (Jarungthammachote & Dutta, 2008; Rupesh et al., 2016). The model demonstrated exceptional simulation performance in attempting to capture the understand of the gasification phenomenon.

3.2. SOFC Model Validation

This SOFC stack model was built using Aspen Plus simulation, and it is based on tubular SOFC technology. Validation of the constructed SOFC model against experimental or validated data sets is required. The model was validated using operational characteristics from Siemens Power Generation Inc.'s model of a 120 kW tubular SOFC stack. Results from both the simulation and the experiment were compared to one another as system outputs. You may find a summary of the SOFC's operational parameters in Table 11.

Table 11. Operating conditions of the model

Parameters	**Values**
Fuel inlet composition (%, mole)	CH_4 81.3%, N_2 14.3%, CO 0.9%, C_4H_{10} 0.2%, C_2H_6 2.9%, C_3H_8 0.4%,
Active Area (m^2)	96.1
DC_{power} output (kW)	120
SOFC Operating Temperature (°C)	910
SOFC Operating Pressure (bar)	1.08
Inlet Fuel Temperature (°C)	200
Inlet Air Temperature (°C)	630
Cell Number	1152
Ua	0.19
Uf	0.85
DC to AC inverter efficiency (%)	92
P_{FUEL}/P_{SOFC}	3

Thermal Losses	2%
Steam to carbon ratio	2.5

Similar to the experimental work, the system's working parameters were adjusted, and fuel was defined with specified composition in Table 11. Current density, cell voltage, gross AC efficiency, and other operatinfg parameters at the respective streams were used to evaluate the outputs. Table 12 displays the resulting comparisons.

Table 12. Comparison of SOFC results for our model and literature studies

Parameters	**Experimental (Veyo & Lundberg, 1999)**	**Model (Doherty, 2014)**	**Our Model**
Current Density (mA/cm^2)	180	182.86	189
Voltage (mV)	Not Available	683	683
Cathode Inlet Temperature (°C)	Not Available	823	826
Pre-reforming Temperature (°C)	550	535	544
Exhaust Temperature (°C)	847	833	836
Anode Inlet Gas Composition (%, mole)	Not Available	5.6% CO, 6.2% N_2, 27.8% H_2O, 23.1% CO_2, 10.4% CH_4, 26.9% H_2,	5.6% CO, 6.2% N_2, 27.8% H_2O, 23.1% CO_2, 10.4%CH_4, 26.9% H_2,
Anode Exhaust Gas Composition (%, mole)	5.0% N_2, 48.0% H_2O,	5.1% N_2, 50.9% H_2O,	5.1% N_2, 50.8% H_2O,

	14.0% H_2, 28.0% CO_2, 5.0% CO	11.6% H_2, 24.9% CO_2, 7.4% CO	11.6% H_2, 24.9% CO_2, 7.4% CO
Gross AC Efficiency (%, LHV)	**50.00**	**51.28**	**51.19**

The model's predictions were quite consistent with the observed data. While there are some minor discrepancies in the model's composition and temperature readings, the model's performance was excellent based on current density, AC efficiency and voltage.

3.3. Evaluation of Operating Parameters on System Performance

3.3.1. Impact of Gasifier Temprature on Syngas Composition

The gasification part's operating temperature is a key factor in determining syngas composition and quality. Most of the equilibrium processes that take place during gasification are endothermic, therefore temperature has a huge impact on the whole process. Generally, fluidized bed reactors used in the biomass gasification process run at temperatures much below 1000 °C to preserve the integrity of the ash produced in the process. In this study, we analyze the effect of gasification temperature on syngas composition using the sensitivity analysis feature of the Aspen Plus simulator. Simulation findings for the concentration changes of H_2, CH_4, CO and CO_2 as a function of temperature are shown in Figure 2; this study was run with the steam to biomass ratio held constant at 0.8.

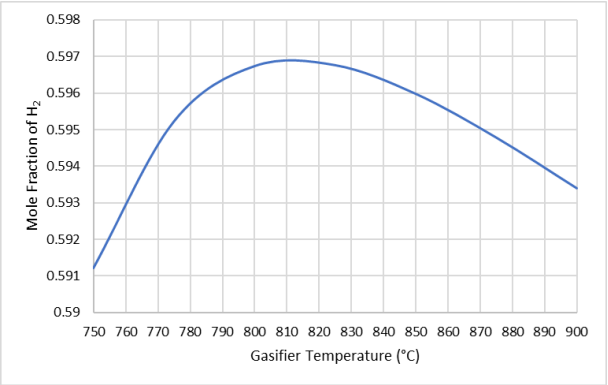

(a)

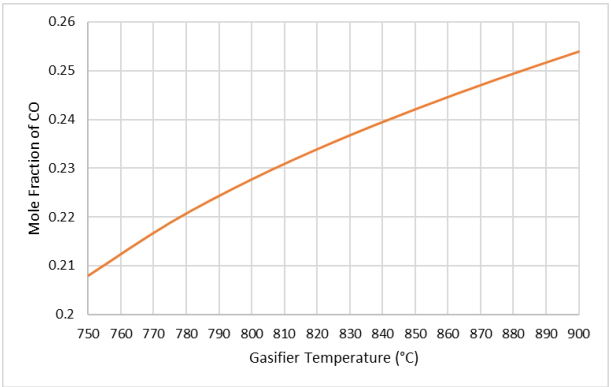

(b)

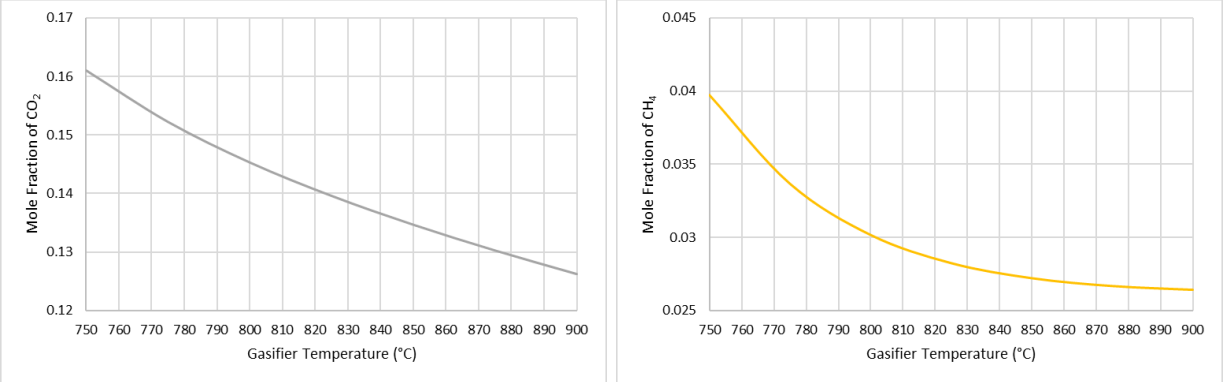

(c) (d)

Figure 2. Impact of gasification step temperature on syngas composition: a) H_2, b) CO, c) CO_2 and d) CH_4

As can be seen in Figure 2, the gasification temperature has a direct impact on the state of chemical equilibrium of the reactions and the syngas composition due to the presence of endothermic and exothermic reactions. According to Le Chatelier's principle, as the temperature is increased, the chemical equilibrium shifts toward the reactant side for exothermic reactions and toward the product side for endothermic reactions (Shehzad et al., 2016).

The H_2 concentration in syngas showed a slight increase, which rose from 59.12% to 59.68%, at a temperature between 750 and 825 °C. The endothermic steam-methane reforming process raised the amount of H_2 gas in syngas while decreasing the amount of CO gas (Pang et al., 2020). Because of Le Chatelier's principle, when the mole fractions of H_2 and CO in syngas increase, the water-gas shift, an exothermic process, moves to the reactant side. Furthermore, the Boudouard reaction, which generates CO and lowers CO_2 at quite high temperatures (>800 °C), is also favored by increasing temperatures. The data showed that when temperature increased, CO concentration rose from 20.80% to 25.30% while CO_2 concentration fell from 16.10% to 12.62%. According to the existing literature, these findings are consistent with expectations (Kartal & Özveren, 2020; Sezer & Özveren, 2021).

3.3.2. Impact of Gasification Step Temprature on SOFC

It is crucial to choose the right parameters to indicate overall system performance when assessing the system based on gasification step temperature. Since syngas composition fluctuated dramatically with gasification temperature, it was believed that this was the most important

parameter in the integrated system. Directly or indirectly, the composition of the syngas and the molar flow are used to determine the SOFC's performance characteristics (electrical efficiency, voltage and current density). With the S/B and anode temperatures held constant at 0.8 and 910 °C, respectively, the impact of gasification step temperature on SOFC evaluation parameters was studied. The findings can be seen in Figure 3.

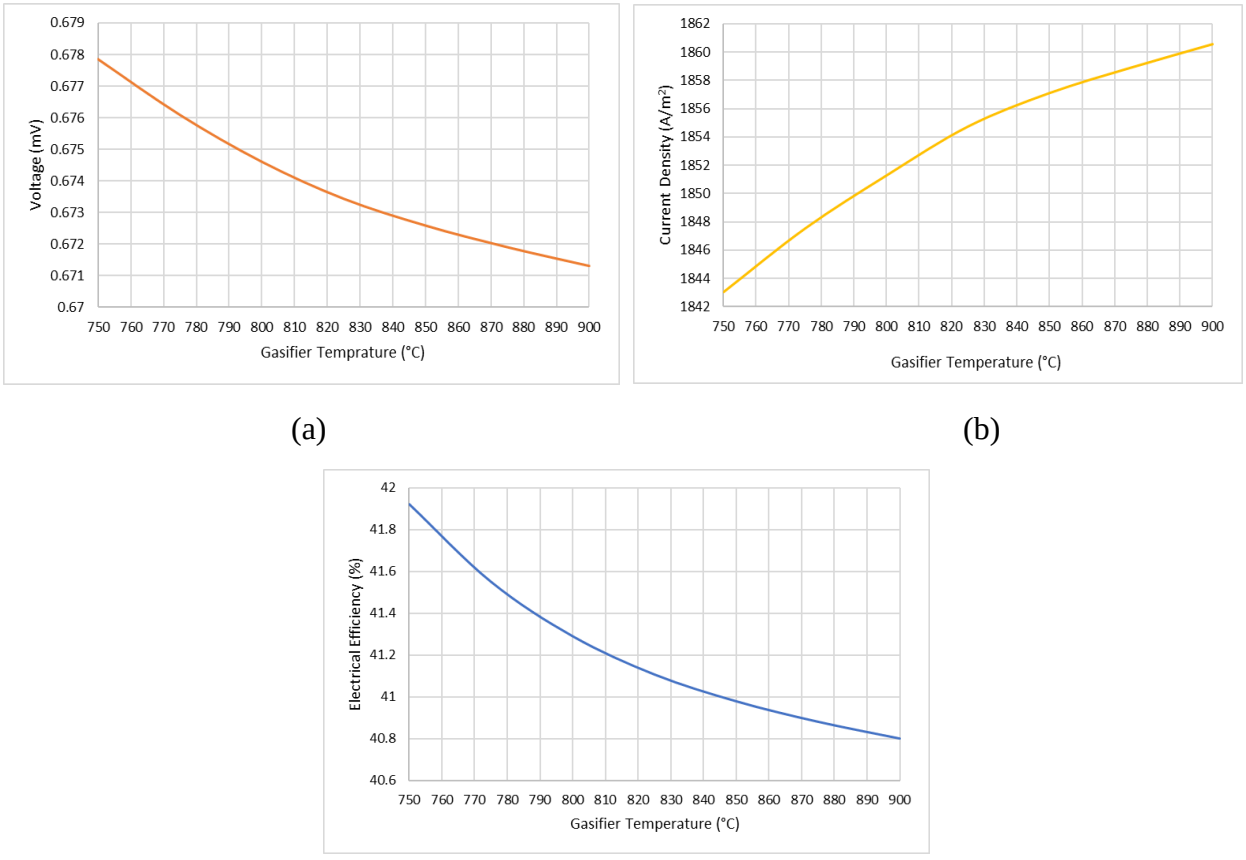

Figure 3. Impact of gasification step temperature on SOFC performance: a) voltage, b) current density, c) electrical efficiency

Figure 3.c shows how the temperature of the gasification step affects the electrical efficiency of the SOFC. As the temperature grew from 750 to 900 °C, the electrical efficiency steadily dropped from 42.92% to 40.80%. Syngas's CH_4 content changed drastically, which corresponded to a drastic decrease in electrical efficiency and voltage. Because it aids in conducting the anode reaction and yields 3 moles of H_2 every cycle, CH_4 reforming is attractive. Rising the operating temperature of the reformer facilitates the reverse water–gas shift reaction at higher temperatures

due to the previously noted decrease in CH_4 content in syngas with increasing temperatures. Since the anode inflow stream contains more and more H_2O due to the reverse water-gas shift reaction, this explains the declining trend in electrical efficiency. Tar in syngas may be generated at lower temperatures, therefore this should be considered even if increasing the temperature did not improve electrical efficiency. This resulted in a doubling of the current density to 120 kW DCP. Figure 3.a shows a decrease in voltage due to voltage losses calculated as a function of increasing current density. This is discussed in detail in subsection 2.2.2.1. Consistency with the findings found in the literature was shown (Abuadala, 2010; Bellomare & Rokni, 2013; Dey et al., 2014; Hosseinpour et al., 2018).

3.3.3. Impact of Steam to Biomass Ratio on Syngas Composition

In terms of syngas composition, the steam to biomass ratio (S/B) is a critical variable. The ratio of the mass flow rate of steam to the feed rate of biomass is named as S/B ratio. Figure 4 displays the findings on the influence of S/B on syngas gas concentrations. When the gasifier temperature was set at 850 °C, a measurement range of 0.5 to 1.0 was chosen for S/B.

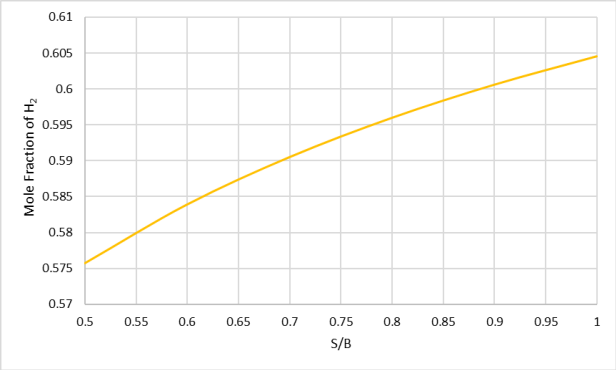

(a)

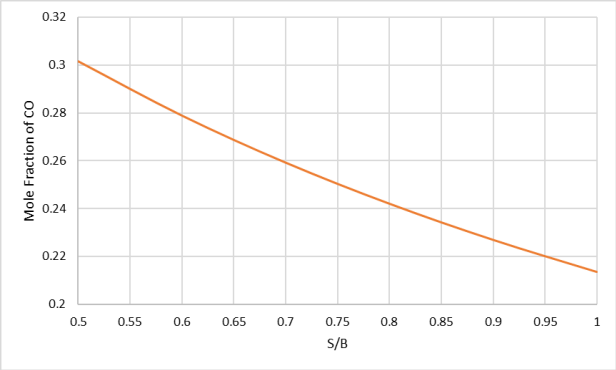

(b)

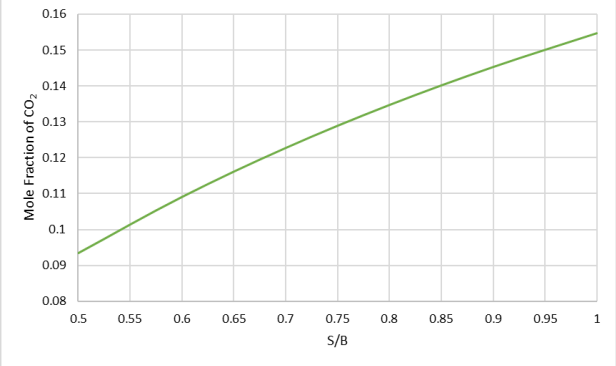

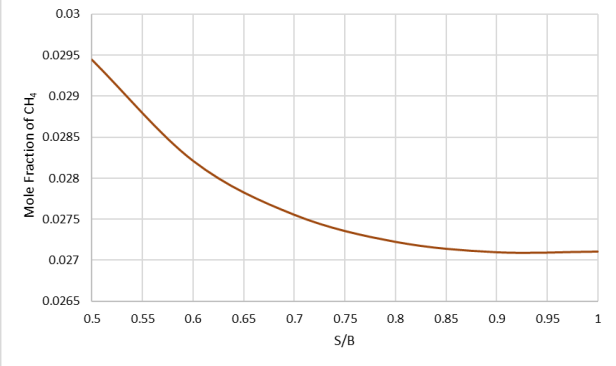

(c) (d)

Figure 4. Impact of S/B on syngas composition: a) H_2, b) CO, c) CO_2 and d) CH_4

When steam is introduced to a gasifier, the partial pressure of H_2O rises. Figure 4 illustrates how the forward processes of water-gas shift, water gas and steam methane reforming reactions are substantially accelerated by the larger partial pressure of H_2O. This action decreased CO_2 and CH_4 emissions while increasing H_2 and CO_2 output. The H_2 content dramatically rose from 57.57% to 60.46%. Unfortunately, adding steam raised CO_2 levels while lowering CO levels as consistent with the literature (Monteiro et al., 2017; Sezer et al., 2021). Therefore, it is crucial to choose the best possible value to produce syngas rich in H_2 and low in CO_2.

3.3.4. Impact of S/B on SOFC

While SOFCs can tolerate certain impurities in the fuel, the efficiency and output of electricity generated from them improves significantly when the H_2 percentage of the fuel is increased. As was discussed in the introduction, steam is a crucial factor in determining the precise composition of syngas. Parameters of SOFC performance were measured as a function of S/B as presented in Figure 5. As part of the parametric analysis, we held the temperatures of the gasification phase and the SOFC anode constant at 850 °C and 910 °C, respectively.

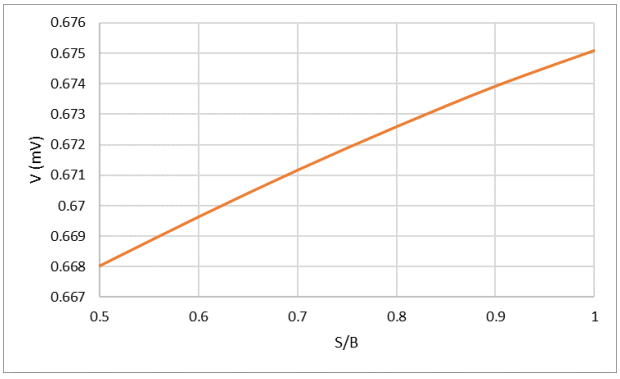

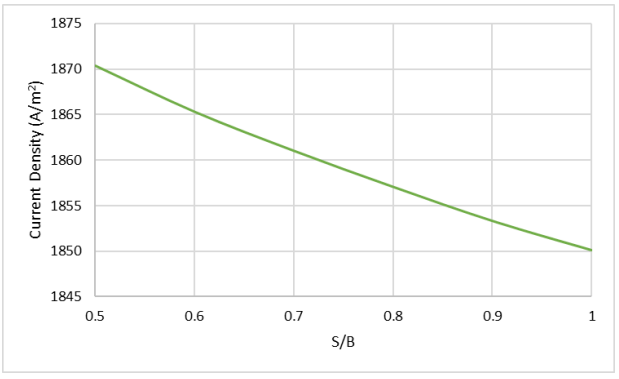

(a) (b)

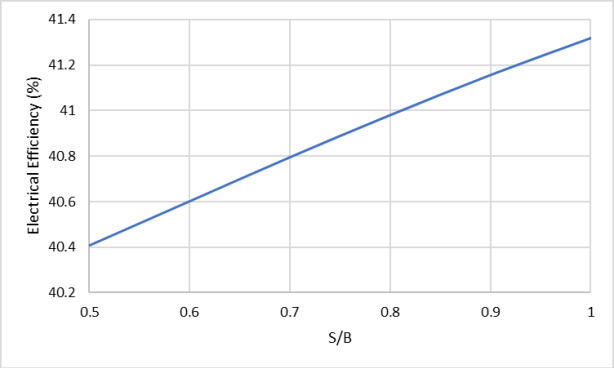

(c)

Figure 5. Impact of S/B on SOFC performance: a) voltage, b) current density, c) electrical efficiency

The influence of S/B on the concentration of syngas was demonstrated in the previous section, where it was established that the amount of CO_2 and H_2 rose in the produced gas with an enhancing ratio of steam. In addition, enhancing H_2 amount around 4.00% promoted the electrochemical reactions in anode. Figure 5.a shows that when the H_2 partial pressure at the anode inlet was raised, the voltage value also rose. The improved voltage results from a reduction in voltage losses made possible by the increase in current density. Thus, as shown in Figure 5.c, the electrical efficiency of SOFC rose from 40.41% to 41.32%. The results gained followed a trend that was seen in the existing literature (Sezer et al., 2022).

3.3.5. Impact of Anode Temperature on SOFC

Anode is the primary site of electrochemical processes. It is crucial to evaluate the influence of anode temperature on SOFC performance, since the pace of the reaction is highly affected by temperature. Anode working temperature was altered among 900 and 980 °C while S/B and gasification part temperature were kept stable at 0.8 and 850 °C, respectively. Voltage, electrical efficiency, and current density are used as evaluation parameters for SOFCs, and they are all shown to be affected by the anode temperature in Figure 6.

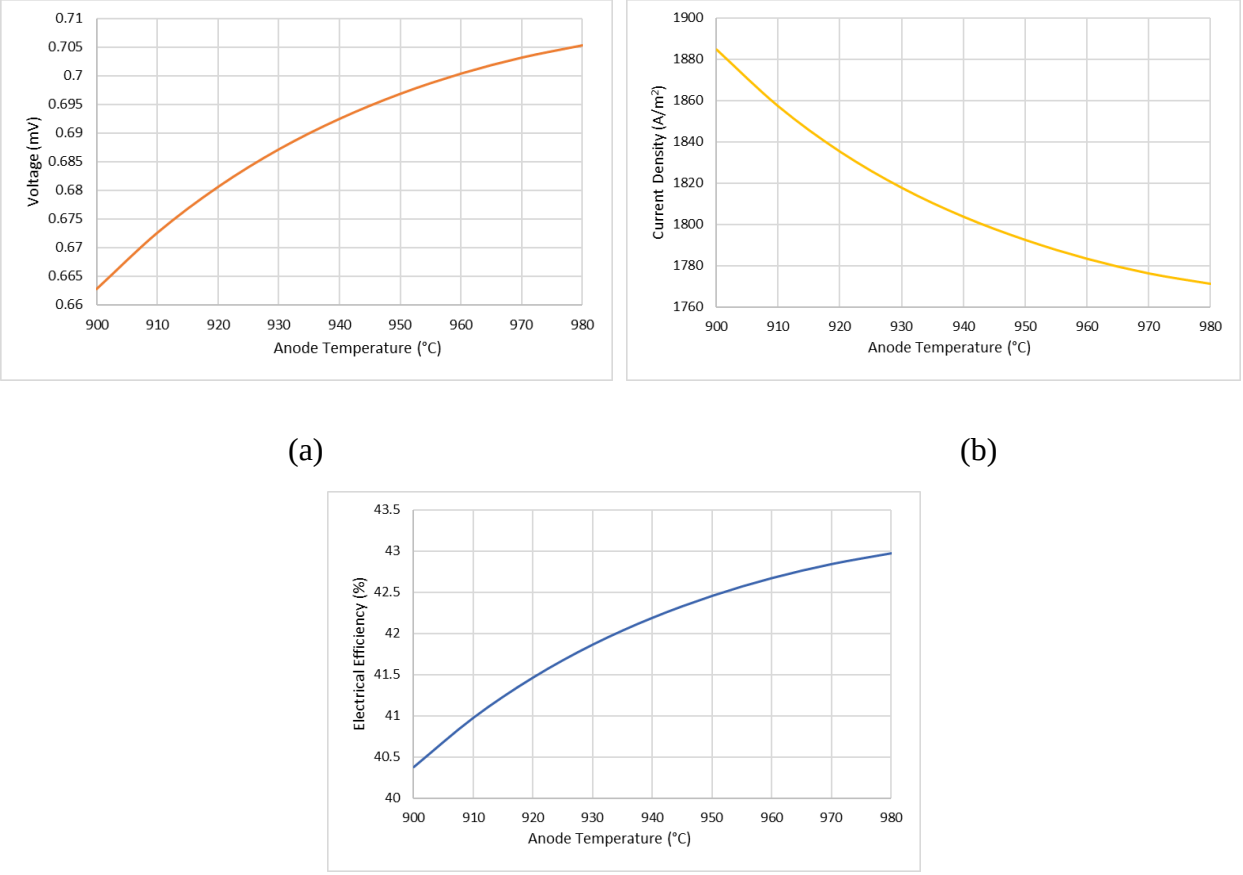

Figure 6. Impact of anode operating temperature on SOFC performance: a) voltage, b) current density, c) electrical efficiency

Increasing the SOFC's working temperature increases the rate of the electrochemical processes, which in turn improves the electrical efficiency, as shown in Figure 6.a. Significant progress was made in electricity efficiency, jumping from 40.38% to 42.98%. Because of this, more O_2 is being drawn into the anode region as the rate of electrochemical reactions rises. The increase in O_2 partial pressure improved voltage since it resulted in less current density and fewer voltage losses. High-temperature SOFCs need a more durable material than their low-temperature counterparts, despite the fact that their performance improved dramatically at higher temperatures. As a result, the cost of high-resistance materials and upkeep time should be minimized by optimizing the temperature of SOFCs.

Conclusion

In this study, the microalgae biomass sample was used as the fuel source for gasification with integrated SOFC system. Research in both theory and experiment has confirmed the accuracy of the Aspen Plus model of the bubbling bed gasifier with integrated SOFC. Sensitivity analysis study findings shown that operating temperatures and S/B had substantial effects on syngas composition. Produced gas from microalga gasification was reached high content of H_2 (60%) with steam addition. As the temperature climbed from 750 to 900 °C, a large fall in CH_4 concentration resulted in a gradual decline in electrical efficiency, from 42.92% to 40.80%. The influence of S/B on the composition of produced gas was demonstrated. The electrical efficiency of SOFC increased from 40.41% to 41.32% when the H_2 concentration was raised to roughly 4.00%, which aided the electrochemical processes in the anode. The another important parameter anode operatint temperature showed highly positive impact on SOFC. The electrical efficiency jumped from 40.38% to 42.98%.

References

Abuadala, A. G. (2010). *Investigation of sustainable hydrogen production from steam biomass gasification* [PhD Thesis, University of Ontario Institute of Technology]. Canada.

Ahmed, T. Y., Ahmad, M. M., Yusup, S., Inayat, A., & Khan, Z. (2012). Mathematical and computational approaches for design of biomass gasification for hydrogen production: A review. *Renewable and Sustainable Energy Reviews*, *16*(4), 2304-2315.

Baruah, D., & Baruah, D. (2014). Modeling of biomass gasification: A review. *Renewable and Sustainable Energy Reviews*, *39*, 806-815.

Basu, P. (2018). *Biomass gasification, pyrolysis and torrefaction: practical design and theory*. Academic press.

Bellomare, F., & Rokni, M. (2013). Integration of a municipal solid waste gasification plant with solid oxide fuel cell and gas turbine. *Renewable Energy*, *55*, 490-500.

Celaya, A. M., Lade, A. T., & Goldfarb, J. L. (2015). Co-combustion of brewer's spent grains and Illinois No. 6 coal: Impact of blend ratio on pyrolysis and oxidation behavior. *Fuel Processing Technology*, *129*, 39-51.

Chen, C., Ma, X., & Liu, K. (2011). Thermogravimetric analysis of microalgae combustion under different oxygen supply concentrations. *Applied Energy*, *88*(9), 3189-3196.

Chisti, Y. (2007). Biodiesel from Microalgae. Biotecnology Advances, 25,294-306. In: Google Scholar.

Dey, T., Singdeo, D., Pophale, A., Bose, M., & Ghosh, P. C. (2014). SOFC power generation system by bio-gasification. *Energy Procedia*, *54*, 748-755.

Doherty, W. (2014). *Modelling of biomass gasification integrated with a solid oxide fuel cell system* [PhD Thesis, Technological University Dublin]. Dublin.

Doherty, W., Reynolds, A., & Kennedy, D. (2010). Computer simulation of a biomass gasification-solid oxide fuel cell power system using Aspen Plus. *Energy*, *35*(12), 4545-4555.

Faraji, M., & Saidi, M. (2021). Hydrogen-rich syngas production via integrated configuration of pyrolysis and air gasification processes of various algal biomass: process simulation and evaluation using Aspen Plus software. *International Journal of Hydrogen Energy*, *46*(36), 18844-18856.

Gómez-Barea, A., & Leckner, B. (2010). Modeling of biomass gasification in fluidized bed. *Progress in energy and combustion science*, *36*(4), 444-509.

Hauck, M., Herrmann, S., & Spliethoff, H. (2017). Simulation of a reversible SOFC with Aspen Plus. *International Journal of Hydrogen Energy*, *42*(15), 10329-10340.

Hosseinpour, J., Chitsaz, A., Eisavi, B., & Yari, M. (2018). Investigation on performance of an integrated SOFC-Goswami system using wood gasification. *Energy*, *148*, 614-628.

Indrawan, N. (2018). *Advanced Biopower Generation Via Gasification of Biomass and Municipal Solid Waste*

Jarungthammachote, S., & Dutta, A. (2008). Equilibrium modeling of gasification: Gibbs free energy minimization approach and its application to spouted bed and spout-fluid bed gasifiers. *Energy conversión and management*, *49*(6), 1345-1356.

Kartal, F., & Özveren, U. (2020). A deep learning approach for prediction of syngas lower heating value from CFB gasifier in Aspen plus®. *Energy*, *209*, 118457.

Lan, W., Chen, G., Zhu, X., Wang, X., Liu, C., & Xu, B. (2018). Biomass gasification-gas turbine combustion for power generation system model based on ASPEN PLUS. *Science of the total environment*, *628*, 1278-1286.

Liu, Y.-Q., Lim, L. R., Wang, J., Yan, R., & Mahakhant, A. (2012). Investigation on Pyrolysis of Microalgae Botryococcus braunii and Hapalosiphon sp. *Industrial & engineering chemistry research*, *51*(31), 10320-10326.

Loha, C., Chattopadhyay, H., & Chatterjee, P. K. (2013). Energy generation from fluidized bed gasification of rice husk. *Journal of renewable and sustainable energy*, *5*(4), 043111.

López-González, D., Fernandez-Lopez, M., Valverde, J., & Sanchez-Silva, L. (2014). Kinetic analysis and thermal characterization of the microalgae combustion process by thermal analysis coupled to mass spectrometry. *Applied Energy*, *114*, 227-237.

Lv, P., Chang, J., Xiong, Z., Huang, H., Wu, C., Chen, Y., & Zhu, J. (2003). Biomass air− steam gasification in a fluidized bed to produce hydrogen-rich gas. *Energy & Fuels*, *17*(3), 677-682.

Monteiro, E., Ismail, T. M., Ramos, A., Abd El-Salam, M., Brito, P., & Rouboa, A. (2017). Assessment of the miscanthus gasification in a semi-industrial gasifier using a CFD model. *Applied Thermal Engineering*, *123*, 448-457.

Motta, I. L., Miranda, N. T., Maciel Filho, R., & Maciel, M. R. W. (2019). Sugarcane bagasse gasification: Simulation and analysis of different operating parameters, fluidizing media, and gasifier types. *Biomass and Bioenergy*, *122*, 433-445.

O'Hayre, R., Cha, S., Colella, W., & Prinz, F. (2009). Fuel Cell Characterization. In *Fuel Cell Fundamentals* (Second Edition ed., pp. 237-238). John Wiley & Sons, Inc.

Özveren, U. (2013). *Theoretical and experimental investigation of biomass and coal gasification* Marmara Universitesi (Turkey)].

Palomba, V., Prestipino, M., & Galvagno, A. (2017). Tri-generation for industrial applications: Development of a simulation model for a gasification-SOFC based system. *International Journal of Hydrogen Energy*, *42*(46), 27866-27883.

Patra, T. K., & Sheth, P. N. (2015). Biomass gasification models for downdraft gasifier: A state-of-the-art review. *Renewable and Sustainable Energy Reviews*, *50*, 583-593.

Ramos, A., Monteiro, E., & Rouboa, A. (2019). Numerical approaches and comprehensive models for gasification process: A review. *Renewable and Sustainable Energy Reviews*, *110*, 188-206.

Rupesh, S., Muraleedharan, C., & Arun, P. (2016). ASPEN plus modelling of air–steam gasification of biomass with sorbent enabled CO2 capture. *Resource-efficient technologies*, *2*(2), 94-103.

Safarian, S., Saryazdi, S. M. E., Unnthorsson, R., & Richter, C. (2020). Artificial neural network integrated with thermodynamic equilibrium modeling of downdraft biomass gasification-power production plant. *Energy*, *213*, 118800.

Segurado, R., Pereira, S., Correia, D., & Costa, M. (2019). Techno-economic analysis of a trigeneration system based on biomass gasification. *Renewable and Sustainable Energy Reviews*, *103*, 501-514.

Sezer, S., Kartal, F., & Özveren, U. (2021). Prediction of chemical exergy of syngas from downdraft gasifier by means of machine learning. *Thermal Science and Engineering Progress*, *26*, 101031.

Sezer, S., Kartal, F., & Özveren, U. (2022). Artificial Intelligence Approach in Gasification Integrated Solid Oxide Fuel Cell Cycle. *Fuel*, *311*, 122591.

Sezer, S., & Özveren, U. (2021). Investigation of syngas exergy value and hydrogen concentration in syngas from biomass gasification in a bubbling fluidized bed gasifier by using machine learning. *International Journal of Hydrogen Energy*, *46*(39), 20377-20396.

Shayan, E., Zare, V., & Mirzaee, I. (2018). Hydrogen production from biomass gasification; a theoretical comparison of using different gasification agents. *Energy conversión and management*, *159*, 30-41.

Shehzad, A., Bashir, M. J., & Sethupathi, S. (2016). System analysis for synthesis gas (syngas) production in Pakistan from municipal solid waste gasification using a circulating fluidized bed gasifier. *Renewable and Sustainable Energy Reviews*, *60*, 1302-1311.

Silva, I. P., Lima, R. M., Silva, G. F., Ruzene, D. S., & Silva, D. P. (2019). Thermodynamic equilibrium model based on stoichiometric method for biomass gasification: A review of model modifications. *Renewable and Sustainable Energy Reviews*, *114*, 109305.

Song, C. (2002). Fuel processing for low-temperature and high-temperature fuel cells: Challenges, and opportunities for sustainable development in the 21st century. *Catalysis today*, *77*(1-2), 17-49.

Veyo, S. E., & Lundberg, W. L. (1999). Solid oxide fuel cell power system cycles. ASME 1999 international gas turbine and aeroengine congress and exhibition,

Zhang, W., Croiset, E., Douglas, P. L., Fowler, M., & Entchev, E. (2005). Simulation of a tubular solid oxide fuel cell stack using AspenPlusTM unit operation models. *Energy Conversion and Management*, *46*(2), 181-196.

Żogała, A. (2014). Critical analysis of underground coal gasification models. Part I: equilibrium models–literary studies. *Journal of Sustainable Mining*, *13*(1), 22-28.